

Synthesis of Spherical Down- and Up-Conversion NaYF₄-Based Nanophosphors with Tunable Size in Ethylene Glycol without Surfactants or Capping Additives

Nuria O. Nuñez,^[a] Hernán Míguez,^[a] Marta Quintanilla,^[b] Eugenio Cantelar,^[b] Fernando Cussó,^[b] and Manuel Ocaña*^[a]

Keywords: Nanoparticles / Luminescence / Rare earth / Fluorides

A very simple route for the synthesis of spherical down-conversion (DC) and up-conversion (UC) NaYF₄-based nanophosphors is described which consists of a precipitation reaction at rather low temperature (max. 120 °C) from solutions containing sodium fluoride and appropriate Ln precursors in a common solvent (ethylene glycol/water mixtures), without the use of any other additive (complexing agent or surfactant). The role played by the nature of the yttrium precursor and the solvent on the morphological characteristics of the nanoparticles is discussed. The size of the nanospheres,

which crystallized in the cubic α -NaYF₄ phase, could be tuned within the 45–155 nm range by adjusting the reaction parameters (temperature and ethylene glycol/water ratio). The applicability of this method is illustrated for the synthesis of Eu^{III}-doped (DC), Tb^{III}-doped (DC) and Yb^{III}/Er^{III} codoped (UC) NaYF₄ nanophosphors, whose luminescent properties were also analysed.

(© Wiley-VCH Verlag GmbH & Co. KGaA, 69451 Weinheim, Germany, 2008)

Introduction

It is well known that when different solids are doped with lanthanide (Ln) ions, interesting luminescent materials are obtained with important applications in the fields of optoelectronics and biotechnology. Among the investigated systems, those based on sodium yttrium fluoride (NaYF₄) have recently been the subject of tremendous attention because this matrix can be doped with certain Ln cations, such as Eu^{III} or Tb^{III}^[1,2], to yield conventional down-conversion (DC) phosphors, or codoped with ytterbium and erbium to become the most efficient up-conversion (UC) phosphor (emission of light with a lower wavelength than that of the excitation radiation) known today.^[2] As a result of these properties, many promising uses have been suggested for these systems, such as solid-state lasers,^[3] flat-panel displays^[4] and biological labelling,^[5,6] to mention a few. Particularly advantageous is the use of the NaYF₄-based UC nanophosphors as bioprobes, mainly because the low energy IR light is weakly absorbed by biological tissue and causes no damage in biological samples.^[2]

For many of these applications it is highly desirable to have uniform nanoparticles with controlled size and shape, as well as good dispersibility.^[5,7] For this reason, important

research in this field is being conducted to develop synthesis procedures that permit adequate control over the morphological (size and shape) properties of the Ln-doped NaYF₄ particles. Until now, several rather sophisticated approaches can be found in the literature, most of which involve the use of very toxic (trioctylphosphane oxide) and/or high-boiling (octadecene, octylamine) organic solvents,^[1,8–11] complexing agents and surfactants^[5,7,12–14] and/or high reaction temperatures (200–300 °C).

In this paper, we describe a very simple alternative route for the synthesis of spherical DC and UC NaYF₄-based nanophosphors which is based on a precipitation reaction at rather low temperature (60–120 °C) from solutions containing sodium fluoride and appropriate Ln precursors in a common solvent (ethylene glycol (EG)/water mixtures), without the use of any other additive (complexing agent or surfactant). The method also permits the control of the size of the precipitated particles through the adjustment of the reaction parameters (temperature and ethylene glycol/water ratio). To illustrate the applicability of this procedure we have chosen both DC (NaYF₄ doped with Eu^{III} or Tb^{III}) and UC (NaYF₄ codoped with Yb^{III} and Er^{III}) systems, whose luminescent properties were also evaluated.

Results and Discussion

Nanophosphor Preparation

First of all, it must be mentioned that we selected ethylene glycol as the reaction medium because it has been well

[a] Instituto de Ciencia de Materiales de Sevilla, CSIC, Americo Vespucio 49, 41092 Isla de la Cartuja, Sevilla, Spain
E-mail: mjurado@icmse.csic.es

[b] Depto. Física de Materiales, C-IV, Universidad Autónoma de Madrid, Madrid, Spain

documented that it may act not only as a solvent but also as a capping agent for the precipitation of different kinds of nanoparticles.^[15–17] A certain amount of water also had to be admixed to facilitate the dissolution of the NaF, used as the source of both sodium and fluoride ions.

In order to establish the appropriate conditions for the synthesis of uniform colloidal dispersions of the NaYF₄-based nanophosphors, we performed a systematic study of the effects of the nature of the Ln precursors, the aging temperature and the EG/water ratio on the characteristics of the precipitates. For this purpose, we selected as a model system the simpler case of pure NaYF₄ using a Y precursor concentration of 0.02 mol dm⁻³ and a NaF concentration (0.1 mol dm⁻³) slightly above the stoichiometric value (0.08 mol dm⁻³). The results are summarised in Table 1. As is observed, nanoparticles with a spherical shape and narrow size distribution, such as those illustrated in Figure 1 (a) were only obtained when using Y(acac)₃ as precursor and an aging temperature in the 60–120 °C range. When the aging was carried out at room temperature, no significant precipitation was observed, whereas agglomerated spheres with a broad size distribution precipitated at 200 °C. The use of other inorganic Y precursors such as yttrium nitrate always resulted in irregular and agglomerated particles (Figure 1, b). To explain this behaviour we must take into account that, as it has been well documented,^[18] the formation of uniform particles in solution requires separating the nucleation and growth steps through a homogeneous precipitation process, which can be achieved, for example, through a slow release of the corresponding precipitating anions or cations^[18] in the reaction medium. In our system, such conditions cannot be satisfied when using an inorganic salt (nitrate) as the starting Y^{III} compound, since it dissociates completely when dissolved. Therefore a rapid precipitation of NaYF₄ takes place after the addition of the Na⁺ and F⁻ ions because of the low solubility of this phase, which would explain the formation of irregular particles in this case. However, the use of the Y(acac)₃ precursor involves different precipitation kinetics. Thus, after dissolving this chelate complex in EG, the Y^{III} cations remain bound to the acetylacetonate ligands. Therefore, for the precipitation of NaYF₄, these cations must first be liberated from the Y(acac)₃ complex, which happens upon increasing the solution temperature to ≥60 °C, since no significant precipitation took place at room temperature. Our results indicate that such a liberation of Y^{III} cations only occurs with appropriate kinetics in the 60–120 °C range. At higher temperatures (200 °C), the dissociation of the Y(acac)₃ complex

seems to be too fast, which results in a much faster precipitation and the production of polydispersed and aggregated spheres (Table 1).

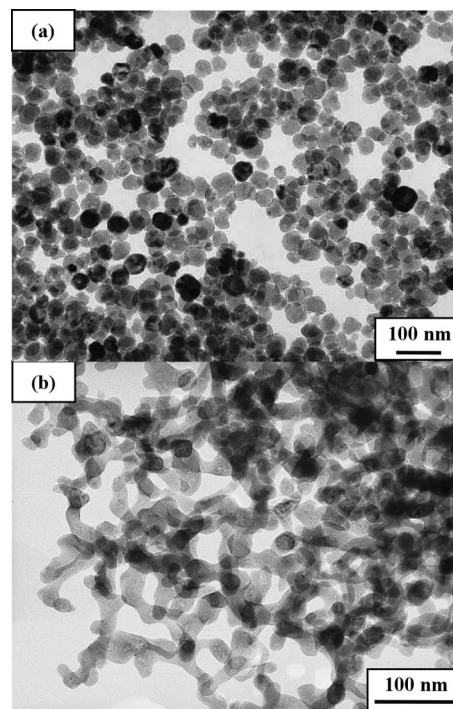


Figure 1. TEM images of the particles obtained from the Y(acac)₃ (a) and Y(NO₃)₃ (b) precursors under the conditions described in the text.

The decrease of the mean particle size from 59 to 45 nm which was detected when the aging temperature was increased from 60 to 120 °C (Table 1) can also be explained according to the above mechanism and the classical theory of nucleation and particle growth.^[19] Thus, the higher the aging temperature, the faster the liberation of Y^{III} cations and therefore NaYF₄ precipitation. Under these conditions a higher number of nuclei must be formed, which should then grow to a smaller size.

It is also important to note that an increase of the mean particle size from 45 to 155 nm was also detected when decreasing the EG/water ratio from 4 to 1 (by volume) (Table 1), which indicates that in our case, EG serves as both solvent and capping agent, as previously observed for other reported systems^[15,16] including YF₃.^[17]

X-ray diffraction revealed that all synthesised samples were crystalline and were formed of the cubic α -NaYF₄

Table 1. Crystallite size and particle shape and size of the NaYF₄ samples obtained at constant NaF concentration (0.1 mol dm⁻³) from different Y precursors (0.02 mol dm⁻³) in different ethylene glycol/water mixtures. The standard deviations are shown in parentheses.

Y ^{III} precursor	EG/H ₂ O, (v/v)	Temperature [°C]	Particle shape	Crystallite size [nm]	Particle size [nm]
Y(acac) ₃	4:1	60	spheres	65	59 (10)
Y(acac) ₃	4:1	120	spheres	54	45 (6)
Y(acac) ₃	4:1	200	spheres	84	agglomerated
Y(acac) ₃	1:1	120	spheres	163	155 (25)
Y(NO ₃) ₃	4:1	120	irregular	–	agglomerated

phase (JCPDS file no. 1-77-2042), as illustrated in Figure 2 for the sample prepared at 120 °C. The crystallite size estimated by using the Scherrer equation was in all cases very similar to the particle size measured from the TEM micrograph (Table 1), which indicates that the precipitated particles were monocrystalline.

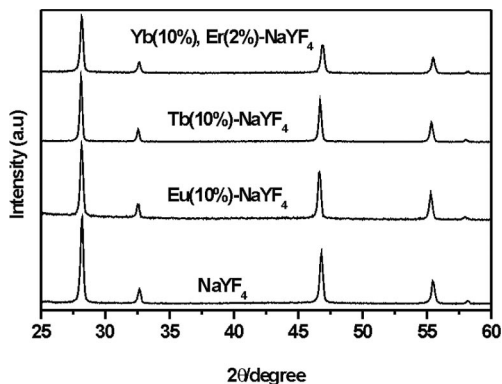


Figure 2. X-ray diffraction patterns for the pure NaYF₄ nanoparticles obtained from Y(acac)₃ and for the Eu^{III}-doped, Tb^{III}-doped and Yb^{III}/Er^{III}-codoped NaYF₄ systems shown in Figure 3.

To obtain the different nanophosphors, we proceeded as described above for the pure NaYF₄ system but with the incorporation of the desired amount of the doping ion precursor to the starting 0.02 mol dm⁻³ Y(acac)₃ solution. For these experiments, we selected an aging temperature of 120 °C and an EG/water ratio of 4 because these conditions led to the smallest NaYF₄ nanospheres (Table 1).

As observed in Figure 3, the most noticeable effect of the addition of 10% (Ln/Y mol ratio) of Eu^{III} or Tb^{III} to the raw Y^{III} solution to prepare DC phosphors was an increase of the mean particle size from 49 to 70 nm (standard deviation: 10 nm) for the former case or to 96 nm (standard deviation: 16 nm) for the latter (Table 2). The same effect was also observed in the preparation of UC phosphors through the simultaneous addition of both 2% of Er^{III} and 10% of Yb^{III} (Figure 3), which resulted in a mean particle size of 67 nm (standard deviation: 9 nm). This behaviour might be due, at least in part, to the higher total concentration of Ln ions used for the composite systems.

EDX spectroscopy evidenced the presence of the doping cations in the phosphor samples. Thus, in the spectra recorded for several single particles of the Eu-doped, Tb-doped or Er/Yb-codoped systems, the peaks corresponding to Eu, Tb or Er and Yb were always detected in addition to those of Na, Y and F (Figure 4). The success of the doping procedure was further confirmed by the XRD patterns of the doped samples (Figure 2), which in all cases only showed the peaks corresponding to the α-NaYF₄ phase. Moreover, the refinement of the unit cell parameters for the case of the Eu- or Tb-doped systems indicated a unit cell expansion (higher for the Eu case) with respect to an undoped NaYF₄ sample (Table 3). This was consistent with the formation of solid solutions by the replacement of some Y^{III} cations with Eu^{III} or Tb^{III} ions in the α-NaYF₄ lattice, since the ionic radius of the doping cations (0.95 Å for Eu^{III}

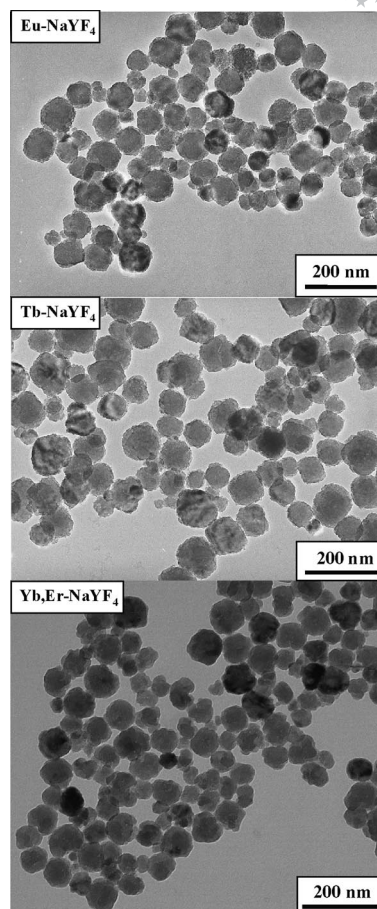


Figure 3. TEM images of the Eu^{III}-doped, Tb^{III}-doped and Yb^{III}/Er^{III}-codoped NaYF₄ nanoparticles whose composition is presented in Table 2.

Table 2. Nominal compositions (molar ratios), crystallite and particle sizes (nm) of the Ln-doped NaYF₄ nanophosphors. The standard deviations are shown in parentheses.

Eu/Y	Tb/Y	Er/Y	Yb/Y	Crystallite size	Particle size
0.1	–	–	–	74	70 (10)
–	0.1	–	–	105	92 (15)
–	–	0.02	0.1	72	67 (9)

and 0.923 Å for Tb^{III}) is higher than that of Y^{III} (0.893 Å).^[20] For the Yb/Er-codoped nanophosphors, the measured unit cell volume was smaller than that of the undoped sample (Table 3), which would be in agreement with the smaller size of the Yb^{III} (0.858 Å) and Er^{III} (0.881 Å) ions,^[20] when compared with that of Y^{III}. However, in this case the observed variation was almost within the experimental error, which is probably because of the smaller difference between the ionic radius of the doping cations and Y^{III}. XRD also suggested that the nanophosphor particles were monocrystalline, as in the undoped samples, since their mean diameter was in all cases very similar to the crystallite size (Table 2).

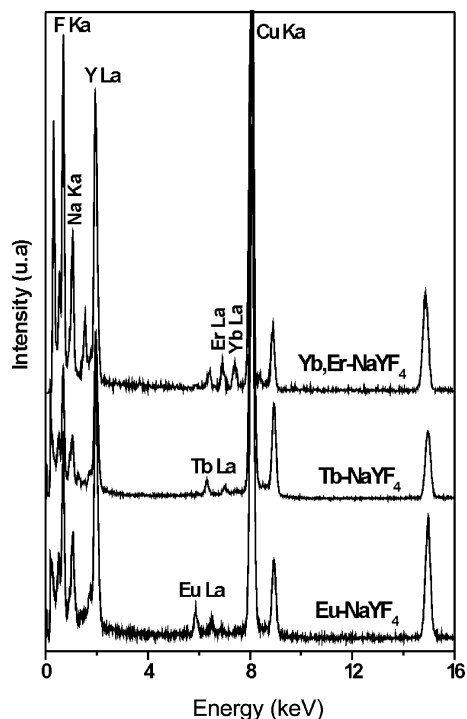


Figure 4. EDX spectra of the Eu^{III}-doped, Tb^{III}-doped and Yb^{III}/Er^{III}-codoped NaYF₄ nanoparticles shown in Figure 3. The most intense peak for each element has been labelled.

Table 3. Unit cell parameters and unit cell volumes measured for the nanophosphors and for an undoped NaYF₄ sample.

Sample	<i>a</i> [Å]	<i>V</i> [Å ³]
NaYF ₄	5.487 ± 0.002	165.20 ± 0.18
Eu(10%)-NaYF ₄	5.497 ± 0.003	166.10 ± 0.27
Tb(10%)-NaYF ₄	5.494 ± 0.003	165.83 ± 0.27
Yb(10%), Er(2%)-NaYF ₄	5.483 ± 0.002	164.83 ± 0.18

Luminescent Properties

The excitation (monitored through the emission at 590 nm) and emission (excitation at 392 nm) spectra recorded for the Eu-doped α -NaYF₄ nanoparticles illustrated in Figure 3 are shown in Figure 5. Both spectra are very similar to those previously reported for pure α -NaEuF₄ nanopolyhedra (5–8 nm) obtained using oleic acid/oleylamine/octadecene mixtures as reaction media,^[1] which is not surprising since the energy of the Eu^{III} levels is hardly affected by the local environment of these ions as a result of the shielding effect of the 5s²5p⁶ electrons. As observed, the excitation spectrum displayed an intense band at 392 nm corresponding to the f–f electronic transitions characteristic of the Eu^{III} ions,^[21] whereas several bands at 575, 590, 611, 649 and 695 nm were detected in the emission spectrum, which are due to the ⁵D₀ → ⁷F_{*J*} (*J* = 0, 1, 2, 3, 4) line emissions of such ions.^[1] The most remarkable difference between the emission spectra of our sample and that reported for the α -NaEuF₄ nanopolyhedra^[1] is that the intensity ratio between the most intense emissions at 575

and 590 nm (*I*₅₉₀/*I*₆₁₁), responsible for the red luminescence of this material, is higher in our case. To explain this behaviour, we must take into account that the ⁵D₀ → ⁷F₁ transition (575 nm) is magnetic-dipole allowed and is insensitive to the local environment of the Eu^{III} cations, whereas the ⁵D₀ → ⁷F₂ transition (611 nm) is significantly affected by the local symmetry around these cations.^[1] Thus, when the local symmetry is lowered, the probability of the ⁵D₀ → ⁷F₂ transition increases, thus increasing the intensity of the 611 nm emission. If we consider that the coordination numbers of the surface cations are lower than those of the bulk, the *I*₅₉₀/*I*₆₁₁ ratio should increase as the number of Eu^{III} cations located at the particle surface decreases. In our nanophosphors, it seems reasonable to assume that the concentration of these ions at the particle surface is very low since, according to the particle formation mechanism discussed above, the Eu^{III} cations which come from an acetate precursor must precipitate faster than the Y^{III} ions coming from the acetylacetonate precursor. As a consequence, the Eu^{III} ions should be mainly located in the core of the particles, which would result in a high *I*₅₉₀/*I*₆₁₁ ratio.

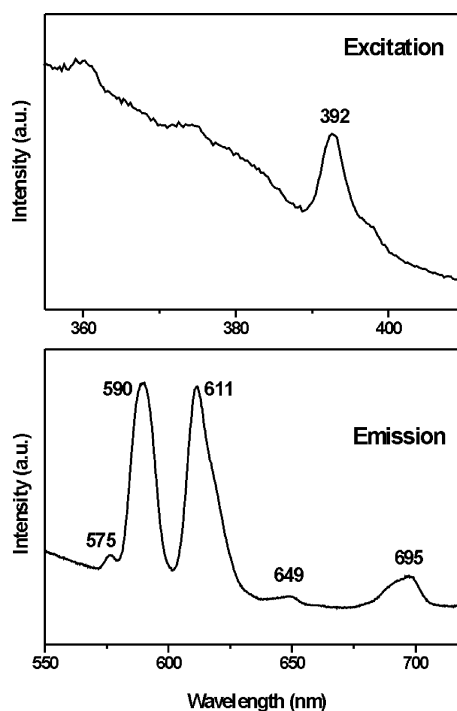


Figure 5. Emission ($\lambda_{\text{ex}} = 392$ nm) and excitation ($\lambda_{\text{em}} = 590$ nm) spectra of the Eu^{III}-doped NaYF₄ nanophosphors.

The excitation (monitored at 542 nm) and emission (excitation at 310 nm) spectra obtained for the Tb-doped α -YNaF₄ nanoparticles illustrated in Figure 3 are shown in Figure 6. As is observed, the emission spectrum displayed three bands at 487, 542 and 583 nm, characteristic of the ⁵D₄ → ⁷F_{*J*} (*J* = 6, 5, 4) transitions of the Tb^{III} ions,^[2,6] which present similar intensities to those previously observed for other Tb^{III}-doped systems^[6] including NaYF₄.^[2]

The sample showed a strong green luminescence as a consequence of the higher intensity of the band appearing at 542 nm.

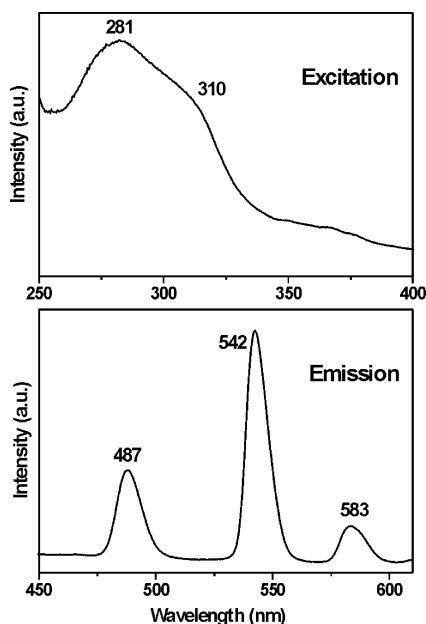


Figure 6. Emission ($\lambda_{\text{ex}} = 310$ nm) and excitation ($\lambda_{\text{em}} = 542$ nm) spectra of the Tb^{III}-doped NaYF₄ nanophosphors.

The success of the doping procedure for the Yb/Er-codoped up-conversion nanophosphors was confirmed by the measurement of their UC properties using two different excitation wavelengths. First, we measured the luminescent properties under direct Er^{III} ion excitation at $\lambda = 785$ nm ($^4I_{15/2} \rightarrow ^4I_{9/2}$ transition). Then, the dominant excitation to the Yb^{III} ions at $\lambda = 980$ nm ($^2F_{7/2} \rightarrow ^2F_{5/2}$)^[22,23] was also studied.

Figure 7 shows the emission spectrum of Yb/Er–NaYF₄ nanophosphors, after direct Er^{III} ion excitation using a laser line at $\lambda = 785$ nm. Two partially overlapping green up-converted emission peaks spanning the spectral range from 520 to 570 nm appeared. These emissions correspond to de-excitations from the $^2H_{11/2}$ and $^4S_{3/2}$ Er^{III} multiplets to the $^4I_{15/2}$ ground state. The excitation mechanism that induces these green emissions involves the sequential absorption of two photons,^[23] as depicted in Figure 8 (a). A first photon induces ground state absorption to the $^4I_{9/2}$ excited state, from where nonradiative relaxation to the metastable $^4I_{13/2}$ level takes place. Then, a second photon causes excited-state absorption to the green-emitting subset of levels. No appreciable additional emission within the visible spectral range is detected.

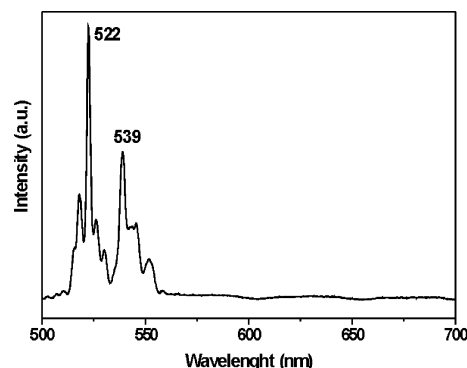


Figure 7. Up-conversion emission spectrum of the Yb^{III}/Er^{III}-codoped NaYF₄ nanophosphors after selective Er^{III} excitation ($\lambda_{\text{ex}} = 785$ nm).

Interestingly, when the Yb/Er–NaYF₄ nanophosphors are excited at $\lambda = 980$ nm, the emission spectrum includes several visible emissions. The UC spectra, obtained for dif-

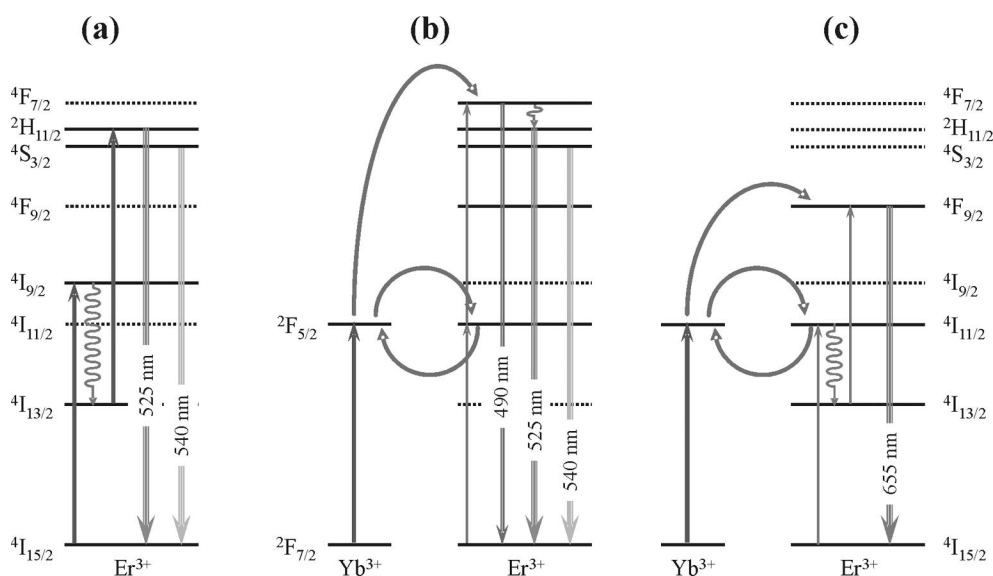


Figure 8. Partial energy level diagram of Yb^{III} and Er^{III} ions, showing the alternative up-conversion excitation mechanisms dependent on the excitation wavelength. (a) Two-photon sequential absorption within Er^{III} ions under $\lambda = 785$ nm. (b) Excited-state energy transfer up-conversion (ETU), $^2F_{5/2} \rightarrow ^2F_{7/2}$ (Yb^{III})/ $^4I_{11/2} \rightarrow ^4F_{7/2}$ (Er^{III}), reaching the $^4F_{7/2}$ upper Er^{III} multiplet. (c) ETU following the $^2F_{5/2} \rightarrow ^2F_{7/2}$ (Yb^{III})/ $^4I_{13/2} \rightarrow ^4F_{9/2}$ (Er^{III}) mechanism that increases the relative intensity of the red emission ($^4F_{9/2} \rightarrow ^4I_{15/2}$ transition).

ferent pump power levels, are shown in Figure 9. In addition to the green emissions, characteristic of the ${}^2\text{H}_{11/2}$, ${}^4\text{S}_{3/2} \rightarrow {}^4\text{I}_{15/2}$ transitions, a strong red emission at around 650 nm and a weaker blue emission at 490 nm are also detected. As it is indicated in Figure 9, these emissions can be associated with the ${}^4\text{F}_{9/2} \rightarrow {}^4\text{I}_{15/2}$ and ${}^4\text{F}_{7/2} \rightarrow {}^4\text{I}_{15/2}$ Er^{III} transitions, respectively. It can also be seen that the spectral shape of the bands, particularly for the green emissions, are strongly dependent on the pump power.

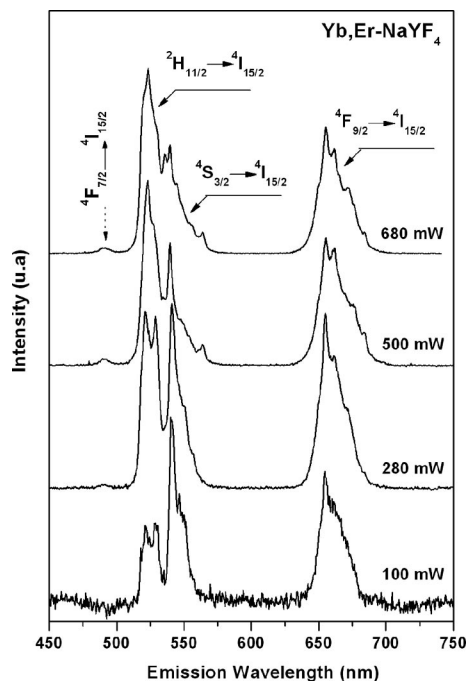


Figure 9. Er^{III} up-converted emission bands measured after Yb^{III} excitation at $\lambda_{\text{ex}} = 980$ nm and different pump power levels.

These spectra can be understood by considering the energy-transfer mechanisms and cooperative up-conversion processes according to the standard description of Er^{III}/Yb^{III}-codoped materials.^[24,25] The excitation wavelength ($\lambda = 980$ nm) is now coincident with the ground-state absorption of Yb^{III} ions (${}^2\text{F}_{7/2} \rightarrow {}^2\text{F}_{5/2}$), with a high absorption cross section, so that it is possible to assume that the pump beam is mainly attenuated by these ions. The ${}^2\text{F}_{5/2}$ Yb^{III} level is energetically resonant with the ${}^4\text{I}_{11/2}$ Er^{III} level, so that efficient energy transfer from Yb^{III} to Er^{III} takes place through the ${}^2\text{F}_{7/2} \rightarrow {}^2\text{F}_{5/2}$ (Yb^{III})/ ${}^4\text{I}_{15/2} \rightarrow {}^4\text{I}_{11/2}$ (Er^{III}) mechanism, as detailed in parts b and c of Figure 8. Then, UC is generated following the absorption of a second excitation photon by Yb^{III} ions and an energy transfer up-conversion (ETU) process, which can take place via two competitive paths.

Figure 8 (b) illustrates how UC proceeds through a second transfer from the Yb^{III} ions following the ${}^2\text{F}_{7/2} \rightarrow {}^2\text{F}_{5/2}$ (Yb^{III})/ ${}^4\text{I}_{11/2} \rightarrow {}^4\text{F}_{7/2}$ (Er^{III}) mechanism. This path populates the green-emitting Er^{III} levels after an intermediate nonradiative relaxation. This mechanism accounts for the (weak) blue emission arising from the ${}^4\text{F}_{7/2}$ (Er^{III}) excited state, which is reached after the second photon absorption.

Alternatively, the Er^{III} ions partially relax nonradiatively from the ${}^4\text{I}_{11/2}$ level to the ${}^4\text{I}_{13/2}$ (Er^{III}) multiplet, from where an ETU process can also take place according to the ${}^2\text{F}_{5/2} \rightarrow {}^2\text{F}_{7/2}$ (Yb^{III})/ ${}^4\text{I}_{13/2} \rightarrow {}^4\text{F}_{9/2}$ (Er^{III}) mechanism, as indicated in Figure 8 (c). This is an excitation path that selectively increases the population of the ${}^4\text{F}_{9/2}$ level, from where the emission band in the red spectral region ($630 \text{ nm} < \lambda < 680 \text{ nm}$) originates. This mechanism accounts for the relative increase of this emission under 980 nm excitation compared with 785 nm excitation.

The change in shape and relative intensities of the green emissions, associated with the ${}^2\text{H}_{11/2} \rightarrow {}^4\text{I}_{15/2}$ and ${}^4\text{S}_{3/2} \rightarrow {}^4\text{I}_{15/2}$ transitions, can be understood by considering that both emitting levels are thermally coupled as a result of the low energy gap between both manifolds. Therefore, the relative intensity of these bands would become affected by temperature changes induced by the energy delivered to the sample by the nonradiative components of the different de-excitation paths: the higher the excitation power, the higher the relative intensity of the high-energy emission (lower wavelength region, at around 525 nm) arising from the ${}^2\text{H}_{11/2}$ level (see Figure 9).

Finally, a first estimation of up-conversion efficiency of our nanophosphors can be made by considering that up-converted green emission can be observed by the naked eye when they are excited by 0.004 W of power at 980 nm with a CW NIR laser (Ti:sapphire) focused to a spot of about 1 mm in diameter. This corresponds roughly to 5 mW/mm² CW power density, not far from the figures reported in the literature for hexagonal nanocrystals.^[26] However, a more precise determination of up-conversion efficiency and transfer (and back-transfer) between Yb and Er ions is currently under progress and will be the subject of a forthcoming paper.

Conclusions

Eu^{III}-doped, Tb^{III}-doped and Yb^{III}/Er^{III}-codoped NaYF₄ spherical nanophosphors can be obtained by precipitating, at low temperatures (60–120 °C), solutions containing sodium fluoride, yttrium acetylacetonate and the appropriate Ln precursors (acetylacetonates or acetates) with ethylene glycol/water mixtures as the solvent. The use of yttrium acetylacetonate as Y precursor is essential to obtain well-dispersed and spherical nanoparticles, since irregular and hard agglomerates result when using other Y sources such as yttrium nitrate. This behaviour is associated with the kinetics of the yttrium acetylacetonate decomposition. The size of the nanospheres, which crystallized in the cubic α -NaYF₄ phase, could be tuned within the 45–155 nm range by adjusting the reaction parameters (temperature and ethylene glycol/water ratio). Irrespective of the doping cation, all samples crystallised in the cubic α -NaYF₄ phase. The Eu-doped and Tb-doped systems displayed strong DC fluorescence with dominant emissions in the red and green regions, respectively, when excited by UV radiation (259 nm for Eu^{III} and 310 nm for Tb^{III}), which is characteristic of

these lanthanide cations. Finally, up-conversion processes in the Er/Yb-codoped nanoparticles have been demonstrated, either through direct excitation to Er ions at $\lambda = 785$ nm or through energy transfer from Yb ions after excitation at $\lambda = 980$ nm. The observed differences in the corresponding emission spectra are in agreement with the standard description of energy transfer in Er^{III}/Yb^{III}-codoped materials which considers two competitive paths of cooperative up-conversion processes.

Experimental Section

Reagents: Yttrium(III) acetylacetonate [Y(CH₃COCHCOCH₃)₃·xH₂O, from Alpha, 99.9%], yttrium(III) nitrate [Y(NO₃)₃·6H₂O, from Aldrich, 99.99%], europium(III) acetate hydrate [Eu(CH₃-COO)₃, from Alfa Aesar], terbium(III) acetylacetonate [Tb(CH₃COCHCOCH₃)₃, from Alfa Aesar, 99.9%], ytterbium(III) acetylacetonate [Yb(CH₃COCHCOCH₃)₃, from Alfa Aesar, 99.9%] and erbium(III) acetylacetonate [Er(CH₃COCHCOCH₃)₃, from Alfa Aesar, 99.9%] were selected as Ln precursors. Sodium fluoride (NaF, Fluka, >99%) was used as the fluoride and sodium source, and ethylene glycol (Fluka, <99.5%) was used as solvent. All chemicals were used as received.

Nanoparticle Synthesis: The standard procedure for the synthesis of the sodium yttrium fluoride nanoparticles was as follows. Proper amounts of the Ln precursors were dissolved in ethylene glycol (2.5 cm³) under magnetic stirring, and the reaction vial was heated at ca. 100 °C to facilitate the dissolution process after which the resulting solution was left to cool down to room temperature. In the same way, the desired amount of NaF was dissolved in water (1 cm³) in a separate vial. After cooling this down to room temperature, ethylene glycol (1.5 cm³) was added to the aqueous solution. The so prepared rare-earth salts and NaF solutions were then mixed under magnetic stirring, and the resulting mixture was quickly introduced into an oven preheated to the desired temperature in which they were finally aged for 5 h in pyrex test tubes tightly closed with screw caps. After aging, the resulting dispersions were cooled down to room temperature, centrifuged to remove the supernatants and washed twice with ethanol. Finally, the nanoparticles were easily dispersed in distilled water. It should also be mentioned that although some sedimentation occurred after 15–20 min, the particles could be resuspended by a slight shaking. For XRD analyses and the measurement of the UC properties, the samples were dried at room temperature.

Characterization: The shape of the nanoparticles was examined by transmission electron microscopy (TEM, Philips 200CM). For this, a droplet of an aqueous suspension of the samples was deposited on a copper grid coated with a transparent polymer and then allowed to dry. The particle size distributions were obtained from the micrographs by counting about one hundred particles.

The qualitative composition of the precipitated particles was assessed by energy-dispersive X-ray analysis (EDX, Philips DX4) coupled to the TEM microscope.

The crystalline structure of the prepared nanoparticles was identified by X-ray diffraction (Siemens D501). The crystallite size was estimated from the most intense XRD peak of the NaYF₄ structure by using the Scherrer method. Unit cell parameters were determined by a least-squares refinement from the X-ray diffraction data collected at intervals of 0.02° (2 θ) for an accumulation time for interval of 10 s, using silicon (20% by weight) as internal standard.

The crystallographic data for the NaYF₄ cubic structure were taken from the JCPDF file number 1-77-2042 reported for this compound.

For the DC systems, the excitation and emission spectra of the samples dispersed in water were measured in a Horiba Jobin Yvon spectrofluorimeter (Fluorolog FL3-11) operating with a 1.5 nm slit. For the UC systems, the optical measurements were performed for powdered pressed samples using a JENOPTIK laser diode source at 980 nm to excite the Yb^{III} ions with different excitation powers. The visible Er^{III} luminescence was dispersed by using an ARC Spectrapro 500-I monochromator and then detected with a photomultiplier tube. The UC properties were also measured with a Horiba Jobin Yvon Raman spectrophotometer (LabRam) attached to a microscope operating in reflection mode. In this case, the excitation wavelength emitted by a solid-state laser with an output power of 300 mW was 785 nm. Pressed powdered samples were irradiated using a 100-fold magnification objective through which the scattered light was also collected. The emitted light was spectrally analysed using a diffraction grating (600 lines/mm) and a CCD detector.

Acknowledgments

This work has been funded by the Ramón Areces Foundation, the Spanish Ministerio de Educación y Ciencia (MEC) under grants ENE2004-01657, MAT2005-03028, MAT2005-05950 and Comunidad de Madrid (MICROSERES S-0505/TIC/0191). N. O. Nuñez and M. Quintanilla want to thank the Spanish Ministerio de Educación y Ciencia for a Juan de la Cierva contract and an FPU grant. We also acknowledge Mr. J. R. Sanchez for his technical assistance in the DC fluorescence measurements.

- [1] H. X. Mai, Y. W. Zhang, R. Si, Z. G. Yan, L. D. Sun, L. P. You, C. H. Yan, *J. Am. Chem. Soc.* **2006**, *128*, 6436.
- [2] L. Wang, Y. Li, *Chem. Mater.* **2007**, *19*, 727.
- [3] T. Sandrock, H. Scheife, E. Heumann, G. Huber, *Opt. Lett.* **1997**, *22*, 808.
- [4] E. Downing, L. Hesselink, J. Ralston, R. Macfarlane, *Science* **1996**, *273*, 1185.
- [5] G. Yi, H. Lu, S. Zhao, Y. Ge, W. Yang, D. Chen, L. Guo, *Nano Lett.* **2004**, *4*, 2191.
- [6] L. Wang, Y. Li, *Chem. Commun.* **2006**, 2557.
- [7] Y. J. Sun, Y. Chen, L. J. Tian, Y. Yu, X. G. Kong, J. W. Zhao, H. Zhang, *Nanotechnology* **2007**, *18*, 275609.
- [8] G. S. Yi, G. M. Chow, *Adv. Funct. Mater.* **2006**, *16*, 2324.
- [9] Y. Wei, F. Lu, X. Zhang, D. Chen, *Chem. Mater.* **2006**, *18*, 5733.
- [10] J. C. Boyer, L. A. Cuccia, J. A. Capobianco, *Nano Lett.* **2007**, *7*, 847.
- [11] J. Shan, X. Qin, N. Yao, Y. Ju, *Nanotechnology* **2007**, *18*, 445607.
- [12] S. Heer, K. Kömpe, H. U. Güdel, M. Haase, *Adv. Mater.* **2004**, *16*, 2102.
- [13] J. H. Zeng, J. Su, Z. H. Li, R. X. Yan, Y. D. Li, *Adv. Mater.* **2005**, *17*, 2119.
- [14] J. H. Zeng, Z. H. Li, J. Su, L. Wang, R. Yan, Y. Li, *Nanotechnology* **2006**, *17*, 3549.
- [15] J. Giri, T. Sriharsha, D. Bahadur, *J. Mater. Chem.* **2004**, *14*, 875.
- [16] N. Pramanik, A. Tarafdar, P. Pramanik, *J. Mater. Process Technol.* **2007**, *184*, 131.
- [17] N. O. Nuñez, M. Ocaña, *Nanotechnology* **2007**, *18*, 455606.
- [18] E. Matijević, *Chem. Mater.* **1993**, *5*, 412.
- [19] V. K. LaMer, *Ind. Eng. Chem.* **1952**, *44*, 1270.

- [20] *Handbook of Chemistry and Physics*, 72nd ed. (Ed.: D. R. Lide), CRC Press, Boston, **1991–1992**, pp. 12–18.
- [21] R. Yan, Y. Li, *Adv. Funct. Mater.* **2005**, *15*, 763.
- [22] N. Menyuk, K. Dwight, J. W. Pierce, *Appl. Phys. Lett.* **1972**, *21*, 159.
- [23] L. Núñez, B. Herreros, R. Duchowicz, G. Lifante, J. O. Tocho, F. Cussó, *J. Lumin.* **1994**, *60–61*, 81.
- [24] L. F. Johnson, H. J. Guggenheim, T. C. Rich, F. W. Ostermayer, *J. Appl. Phys.* **1972**, *43*, 25.
- [25] E. Cantelar, F. Cussó, *J. Lumin.* **2003**, *102–103*, 525.
- [26] G. S. Yi, G. M. Chow, *Adv. Funct. Mater.* **2006**, *16*, 2324.

Received: April 9, 2008

Published Online: June 10, 2008